33RD CONGRESS
OF THE INTERNATIONAL COUNCIL
OF THE AERONAUTICAL SCIENCES
STOCKHOLM, SWEDEN, 4-9 SEPTEMBER, 2022

ICAS 2022 SWEDEN

DESIGN OF AN EFFICIENT CLIMBING FLIGHT TRAJECTORY FOR A FLAPPING-WING MICRO AIR VEHICLE

Sang-Gil Lee[1], Hyeon-Ho Yang[1], Yu-Jeong Han[1] & Jae-Hung Han[1]

[1]Korea Advanced Institute of Science and Technology
Daejeon, 34141, Republic of Korea

Abstract

Flapping-wing micro air vehicles (FWMAVs) have been widely developed to pursue the flight performance of insects. However, the FWMAVs usually have limited flight time. This study aims to increase the flight time by designing energy-efficient trajectory in climbing flight, which is one of the most energy consuming flight modes. The climbing trajectory is designed in 2-dimensional space. The cost function is defined as the energy consumption per unit altitude. Finally, the designed trajectory is converted to the spiral trajectory in 3-dimensional space for climbing flight in a limited flight space.

Keywords: Flapping-wing, Trajectory optimization, Flight trajectory

1. Introduction

Insects in nature have outstanding maneuverability and stability compared with micro air vehicles of humankind. Various flapping-wing micro air vehicles (FWMAV) have been developed to pursue the flight performance of insects. The recently developed FMWAVs have high maneuverability [1] and collision recovery ability [2], however, the endurance of them is usually less than 15 minutes [3].

To increase the flight efficiency of FWMAVs, the aerodynamic force on a flapping wing need to be understood and predicted with moderate accuracy. The unique aerodynamics characteristic of a flapping wing, such as effect of the advance ratio on the lift augmentations [4] and wing-wake interaction [5], have been studied. Also, aerodynamic models, such as the quasi-steady aerodynamic model [6] and unsteady vortex-lattice method (UVLM) [7] have been developed.

Based on the aerodynamic models, many optimization studies have been conducted. Especially, the wing kinematics optimization for hovering [8-10] and forward flight [11] has been the major research subject. However, relatively few studies have been conducted about climbing flight trajectory despite the high energy consumption of climbing flights. The previous studies including Nguyen *et al.* [12] considered the vertical climbing trajectory and did not allow the forward motion. However, the forward motion should be considered because the inflow effect due to the forward motion could be favorable to the climbing flight.

In this study, a trajectory is designed for the climbing flight of FWMAVs. The cost function is defined as energy consumption per unit altitude. The design variables are the pitch command of the designed controller and the flapping frequency. Because the forward motion requires a large open space, the designed 2-dimensional trajectory is converted to the spiral trajectory by maintaining a tilted roll angle with a roll controller. The simulation result of the spiral climbing is compared with the 2-dimensional trajectory.

2. Modeling and simulation environment

2.1 Reference insect and kinematics

In this paper, the hawkmoth is selected as a reference insect. The wing is assumed to be rigid and connected to the body with 3 degrees of freedom (DOF) revolute joint. The morphological and kinematic parameters of the FWMAV are based on the hawkmoth measured by Willmott and Ellington [13].

The wing and body kinematics can be represented using frames of reference. Figure 1 shows three frames of reference. The ground-fixed frame $[x_{\mathrm{G}}\ \mathrm{y_G}\ \mathrm{z_G}]$ is the inertial frame. The body-fixed frame $[x_{\mathrm{b}}\ \mathrm{y_b}\ \mathrm{z_b}]$ is attached to the center of mass of the body, x_{b}-axis points to the head. Stroke plane frame $[x_{\mathrm{sp}}\ \mathrm{y_{sp}}\ \mathrm{z_{sp}}]$ is attached to the wing-base pivot and is used to define the wing kinematics. x_{sp}-axis is on the stroke plane. $\mathrm{y_b}$- and $\mathrm{y_{sp}}$-axes is parallel to the $\mathrm{y_G}$-axis when the insect model is positioned symmetrically.

Wing kinematics are defined with Euler angles. The sequence of rotation is 3-1-2, and the corresponding angles are the sweep angle ϕ_w, the elevation angle θ_w, and the rotation angle α_w (Figure 2). The wing kinematics of the FWMAV are defined by the 3-order Fourier series as shown in Equations (1)-(3) where f is the flapping frequency.

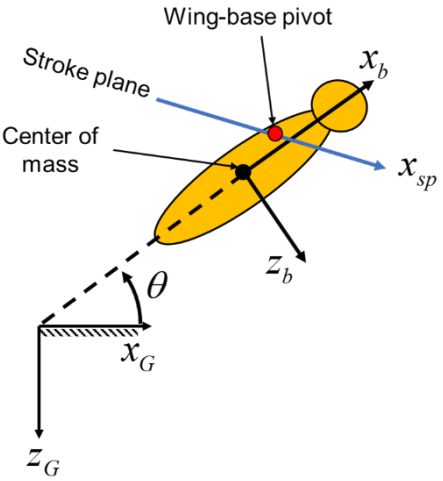

Figure 1 – Frames of reference

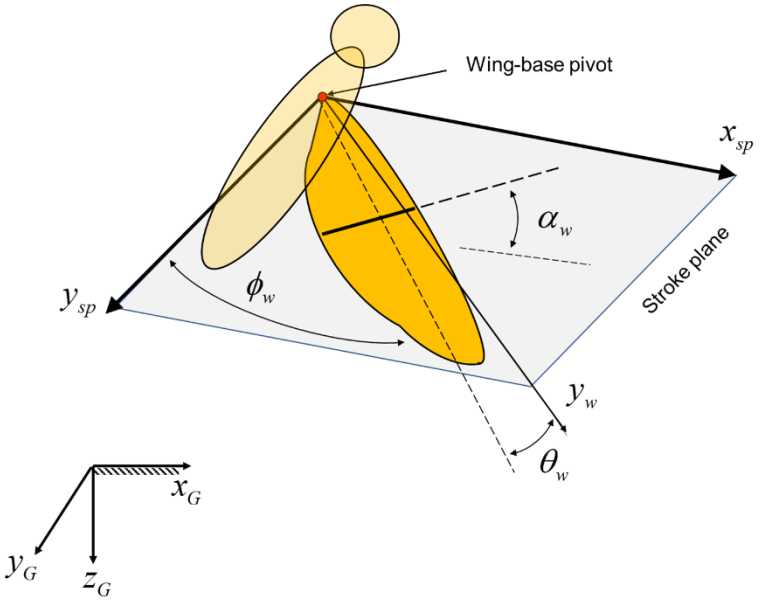

Figure 2 – Wing kinematic angle

$$\phi_w(t) = \frac{\phi_{a_0}}{2} + \sum_{k=1}^{3} ({}_{\phi}a_k \cos(k2\pi ft) + {}_{\phi}b_k \sin(k2\pi ft)) \quad (1)$$

$$\theta_w(t) = \frac{\theta_{a_0}}{2} + \sum_{k=1}^{3} ({}_{\theta}a_k \cos(k2\pi ft) + {}_{\theta}b_k \sin(k2\pi ft)) \quad (2)$$

$$\alpha_w(t) = \frac{\alpha_{a_0}}{2} + \sum_{k=1}^{3} ({}_{\alpha}a_k \cos(k2\pi ft) + {}_{\alpha}b_k \sin(k2\pi ft)) \quad (3)$$

2.2 Simulation environment

The simulation environment consists of two parts: the aerodynamic model and the multi-body dynamics solver.

For the aerodynamic model, the unsteady panel method (UPM) and the extended unsteady vortex-lattice method (UVLM) are used. The UPM is used to compute the aerodynamic force on the body, while the UVLM is applied to the wings. For more details, refer to Nguyen *et al.* [14] This aerodynamic model has moderate fidelity and computational cost.

The nonlinear equations of motion are time-integrated using a commercial multi-body dynamics solver (MSC. Adams). In the MSC. Adams, the equations of the motion are formulated as a set of nonlinear differential-algebraic equations:

$$\mathbf{Q}\ddot{\mathbf{q}} + \boldsymbol{\eta}_{\mathbf{q}}^{T}\boldsymbol{\lambda} - \mathbf{P}^{T}\mathbf{G}(\mathbf{q}, \dot{\mathbf{q}}) = \mathbf{0} \quad (4)$$

$$\boldsymbol{\eta}(\mathbf{q}, t) = \mathbf{0} \quad (5)$$

where $\mathbf{Q}$ is the mass matrix of the system, $\mathbf{q}$ is the vector of coordinates to represent displacement, $\boldsymbol{\eta}$ is the set of the kinematic constraint equations, $\boldsymbol{\lambda}$ is the Lagrange multipliers for constraints, $\mathbf{G}$ is the set of applied forces and gyroscopic terms of the inertia forces where the aerodynamic model is used, $\mathbf{P}^T$ is the matrix that projects $\mathbf{G}$ in $\mathbf{q}$ direction, and $\boldsymbol{\eta}_{\mathbf{q}}$ is the gradient of the constraints at any given states.

3. Trim search

The climbing trajectory can be obtained by increasing flapping frequency from hovering condition while maintaining the pitch angle as the given value. For that, hovering (trim) condition is first obtained and the pitch controller is designed.

3.1 Trim search algorithm

Due to the oscillating aerodynamics, the trim condition about wingbeat-cycle average states $\bar{\mathbf{x}}$ is obtained. $\bar{\mathbf{x}}$ can be calculated as following equation:

$$\bar{\mathbf{x}} = \frac{1}{\mathrm{T}} \int_{\mathrm{T}}^{\mathrm{t+T}} \mathbf{x}\, \mathrm{dt} \quad (6)$$

where T is a flapping period, and the over-bar denotes the wingbeat-cycle average value.

The trim is searched by the iterative algorithm developed by Kim *et al.* [15] The overall flowchart of the trim search process is shown in Figure 3.

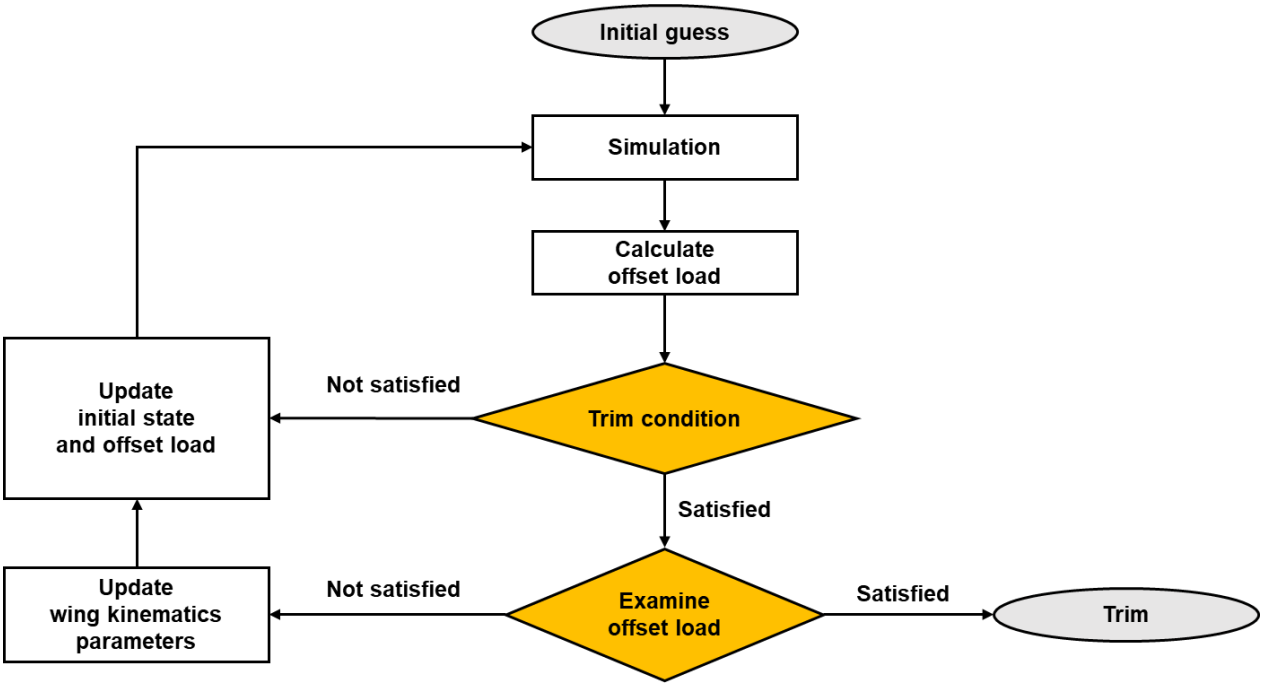

Figure 3 – Flowchart of trim search process

The algorithm determines the parameters of wing kinematics and initial value of states to satisfy the trim criteria:

$$\bar{\mathbf{F}}_{\mathrm{G}} = [\bar{F}_x \quad \bar{F}_y \quad \bar{F}_z]_G = [0 \quad 0 \quad 0] \tag{7}$$

$$\bar{\mathbf{M}}_{\mathrm{G}} = [\bar{M}_x \quad \bar{M}_y \quad \bar{M}_z]_G = [0 \quad 0 \quad 0] \tag{8}$$

$$\bar{\mathbf{x}}_{\mathrm{G}} = [\bar{u} \quad \bar{v} \quad \bar{w} \quad \bar{p} \quad \bar{q} \quad \bar{r}]_G = [u_{\mathrm{given}} \quad 0 \quad 0 \quad 0 \quad 0 \quad 0] \tag{9}$$

where the subscript *G* means that the value is presented in the ground-fixed frame. $\mathbf{F}$, $\mathbf{M}$, and u_{given} are the applied force, the applied moment, and a given forward velocity, respectively. u, v, and w are the velocity components of x-, y-, and z-axes. p, q, and r are the angular rates about x-, y-, and z-axes, respectively.

The obtained hovering condition can be linearized. Eigenvalues of the longitudinal dynamics are shown in Figure 4. The hovering condition is inherently unstable; therefore, a feedback controller is needed.

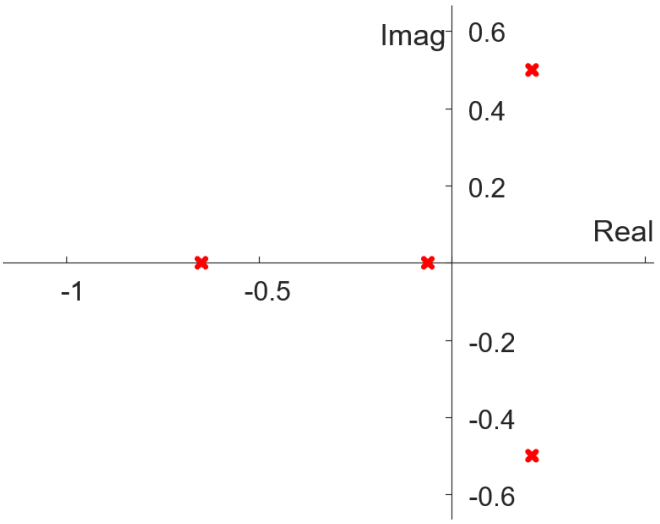

Figure 4 – Eigenvalues of the longitudinal dynamics during hovering flight

3.2 Pitch controller

Pitch angle is controlled by a sweeping bias. The sweeping bias is one of the commonly used control inputs for FWMAVs [16, 17]. The proportional–integral–derivative (PID) controller is designed as

$$\phi_0 = k_1\left(\dot{\theta}_{cmd} - \bar{q}\right) + k_2(\theta_{cmd} - \bar{\theta}) + k_3 \int (\theta_{cmd} - \bar{\theta})\mathrm{dt} \tag{10}$$

where k and θ_{cmd} are control gain and pitch command, respectively.

4. Trajectory design

The cost function is defined as the energy consumption per unit altitude (EPA):

$$J = \frac{\triangle E}{\triangle h} = \frac{\int_{\mathrm{t}}^{\mathrm{t+T}} P \ \mathrm{dt}}{\int_{\mathrm{t}}^{\mathrm{t+T}} w \ \mathrm{dt}} \tag{11}$$

Here, P is a mechanical power consumption as:

$$\begin{aligned} &P = P_{\phi_w} + P_{\theta_w} + P_{\alpha_w} \\ &P_j = \tau_j \frac{dj}{dj} \quad (\tau_j \frac{dj}{dj} > 0) \\ &P_j = 0 \quad (\tau_j \frac{dj}{dj} \leq 0) \\ &(j = \phi_w, \theta_w, \alpha_w) \end{aligned} \tag{12}$$

In this study, it is assumed that the FWMAV does not store the energy in the wings during a period of negative work. A lower EPA means that lower energy is required for increasing the same altitude. The trajectory design problem can be represented by the problem searching design variables (f, θ_{cmd}) that have low cost function (EPA).

Additionally, constraints are need to obtain the feasible trajectory. The upper bound of flapping frequency is set to 7 Hz higher than the hovering frequency, which is about 25% higher than the hovering frequency. The lower bound of pitch command is 0 deg, which means that the body is horizontal. In order avoid too much power consumption, an additional constraint is set so that the power consumption P does not exceed twice that of the cruising flight with 3 m/s forward velocity. Those constraints are represented by following equations:

$$f_{hovering} + 1 \leq f \leq f_{hovering} + 7 \tag{13}$$

$$0 \leq \theta_{cmd} \leq \theta_{hovering} \tag{14}$$

$$P < 2P_{cruise(3m/s)} \tag{15}$$

Because the number of design variables is two, the grid search is conducted. The grid intervals of flapping frequency and pitch command are 1 Hz and 0.2 rad, respectively.

When pitch command is 0 deg, the stroke plane becomes closer to the vertical plane, and it makes the FWMAV unstable due to lower control authority of sweeping bias. Except for the zero-pitch command, the result of the grid search is shown in Figure 5. Lower pitch command and higher frequency results in lower EPA. A lower pitch command leads to a forward motion. Inflow effect due to the forward motion is favorable to lift generation, so it is necessary for efficient climbing trajectory. In Figure 6, the point $(\Delta f = 4\ \mathrm{Hz}, \theta_{cmd} = 10\ \mathrm{deg})$ satisfies the constraints with a margin and is selected as a designed trajectory.

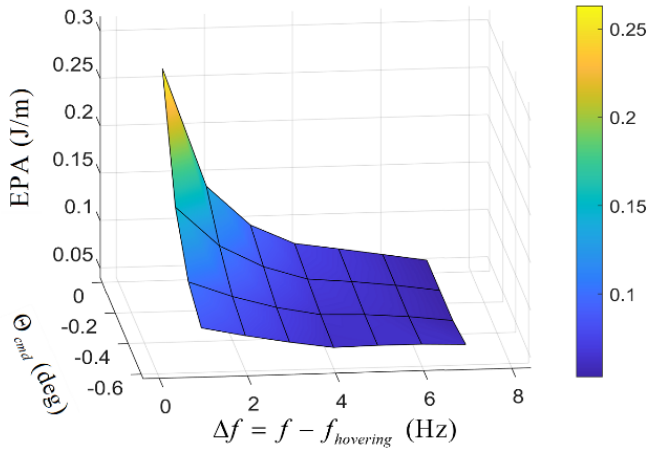

Figure 5 – Energy consumption per unit altitude (EPA)

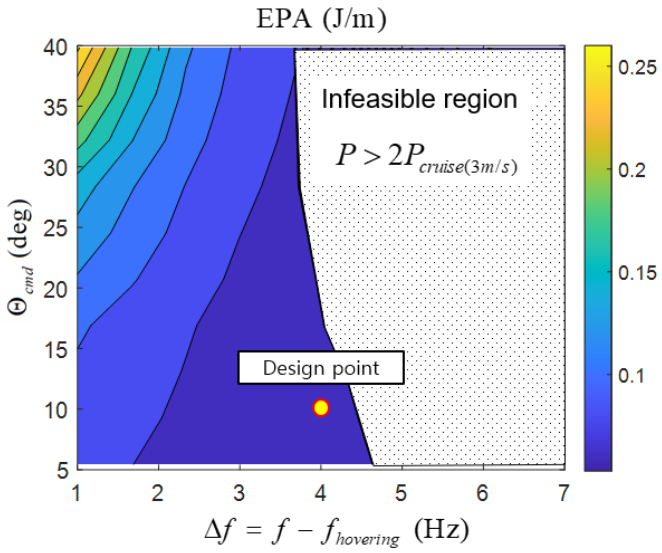

Figure 6 – Designed trajectory

5. Spiral trajectory in 3-dimensional space

The designed 2-dimensional trajectory requires a large open space due to the forward motion. To reduce the required space, the trajectory is converted to the spiral trajectory in 3-dimensional space. The spiral flight can be performed by maintaining a tilted roll angle with a roll controller.

Control inputs of roll controller are $\Delta\phi_{amp}$ and $\Delta\alpha_0$. $\Delta\phi_{amp}$ is the flapping amplitude difference between the right and left wings. $\Delta\alpha_0$ is the mean rotating angle difference between the right and left wings. The effect of these control inputs on rolling moment is illustrated Figure 7.

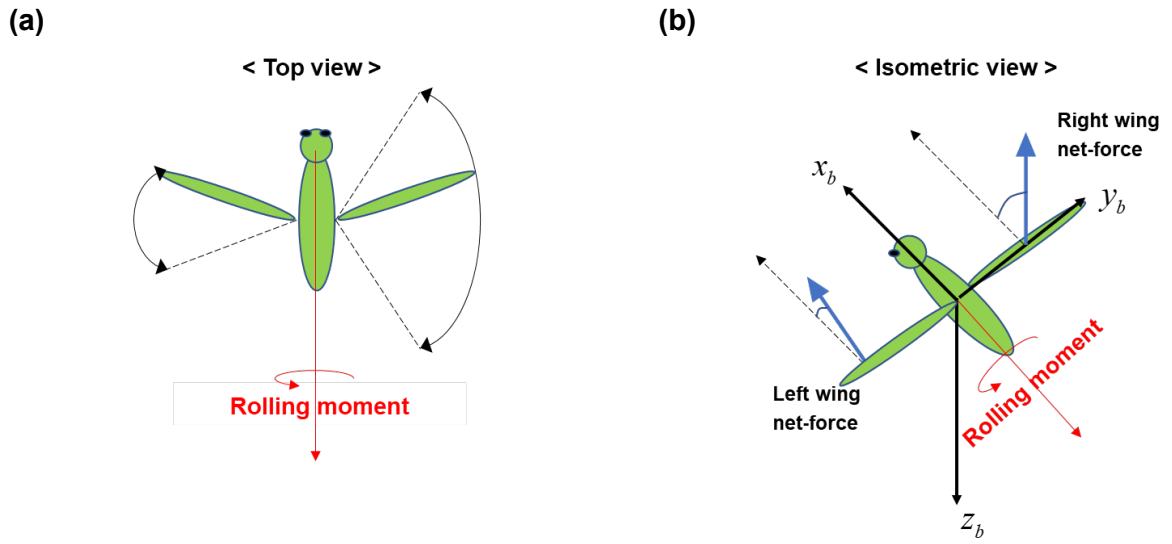

Figure 7 – Effect of (a) $\Delta\phi_{amp}$ and (b) $\Delta\alpha_0$ on rolling moment

The overall control loop is shown in Figure 8, where the pitch command and flapping frequency are the same as the designed trajectory in section 3. The roll command is given as -10 deg.

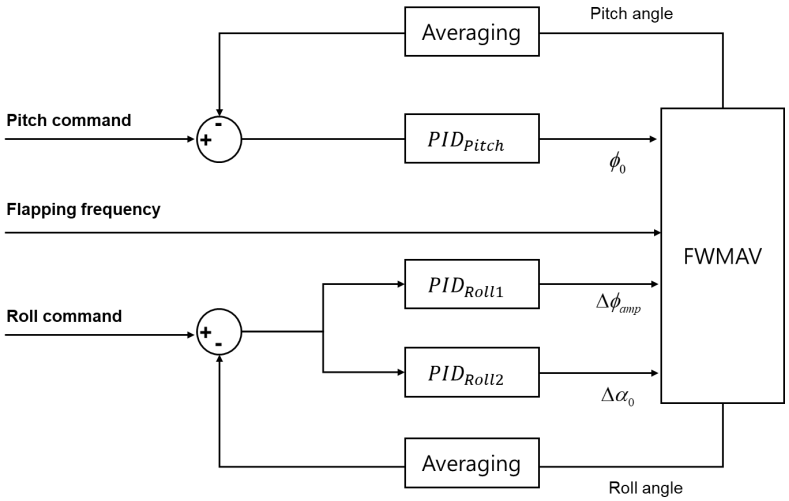

Figure 8 – Controller for spiral flight

Figure 9 shows the roll and yaw angle during the spiral climbing. The designed controller can reach the spiral flight with constant yaw rate and constant roll angle. Figures 10 and 11 show that spiral trajectory require a smaller space and have similar EPA compared to the 2-dimensional trajectory.

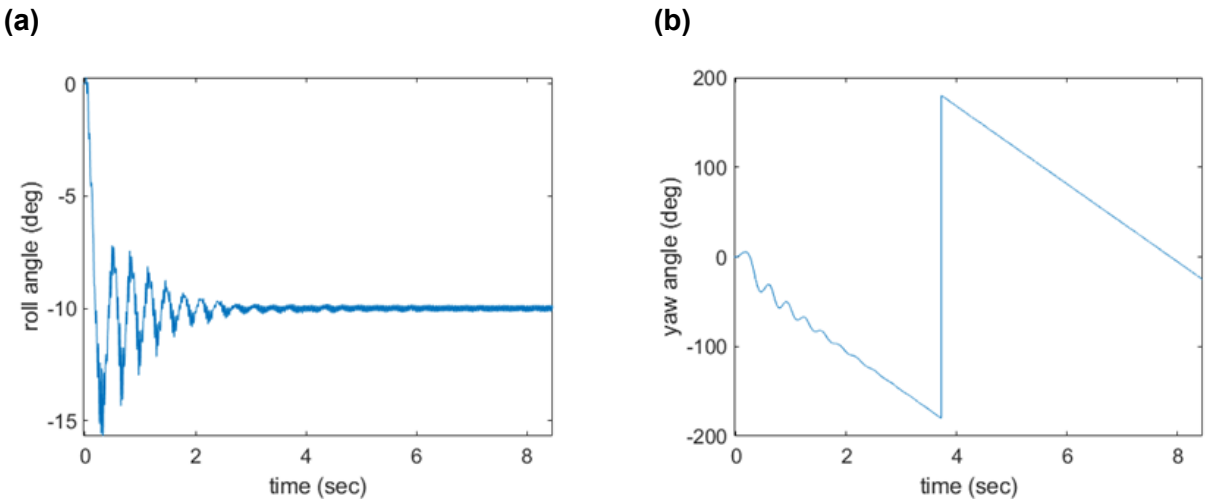

Figure 9 – (a) Roll and (b) yaw angle during the spiral climbing

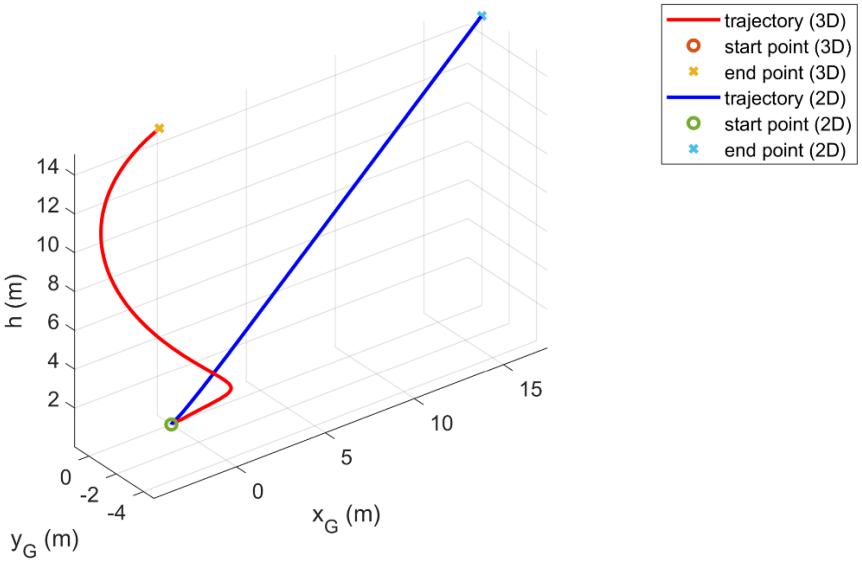

Figure 10 – Trajectory comparison

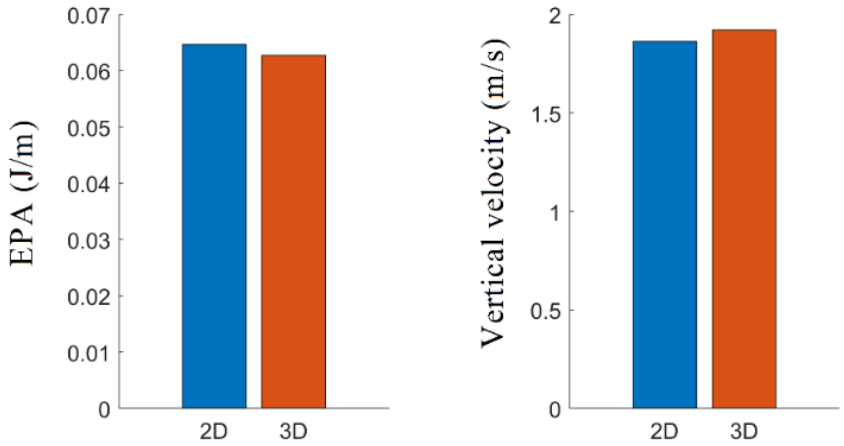

Figure 11 – EPA and vertical velocity Comparison

6. Conclusion

In this study, a flight dynamics model of a hawkmoth-like flapping-wing micro air vehicle (FWMAV) is established and a trajectory design problem is formulated. The simulation model included the UVLM and UPM as an aerodynamic model to consider the wake effect. The trajectory design problem was formulated for the FWMAV to conduct an efficient climbing flight. The cost function was defined as EPA. The design variables were defined as the flapping frequency and pitch command.

The designed 2-dimensional trajectory included the forward motion for efficient lift generation in 2-dimensional space. However, the forward motion required a large open space. The roll controller was designed to reduce the required space. The simulation result with the controller showed the FWMAV can perform the spiral flight with similar EPA to the 2-dimensional trajectory. The presented design process can be utilized for the developed FWMAV to save energy for climbing and increase the flight duration.

7. Acknowledgments

This research was supported by Unmanned Vehicles Core Technology Research and Development Program through the National Research Foundation of Korea (NRF) and Unmanned Vehicle Advanced Research Center (UVARC) funded by the Ministry of Science and ICT, the Republic of Korea (2020M3C1C1A01083415).

8. Contact Author Email Address

Sang-Gil Lee: sanggil.lee@kaist.ac.kr

Hyeon-Ho Yang: hhy9557@kaist.ac.kr

Yu-Jeong Han: yujeong_han@kaist.ac.kr

Jae-Hung Han: jaehunghan@kaist.ac.kr

9. Copyright Statement

10. References

[1] Karásek M, Muijres FT, Wagter CD, Remes BDW, and Croon GCHEd. A tailless aerial robotic flapper reveals that flies use torque coupling in rapid banked turns. *Science,* Vol. 361, No. 6407, pp. 1089-1094, 2018.

[2] Phan HV and Park HC. Mechanisms of collision recovery in flying beetles and flapping-wing robots. *Science,* Vol. 370, No. 6521, pp. 1214-1219, 2020.

[3] Phan HV, Aurecianus S, Au TKL, Kang T, and Park HC. Towards the long-endurance flight of an insect-inspired, tailless, two-winged, flapping-wing flying robot. *IEEE Robotics and Automation Letters,* Vol. 5, No. 4, pp. 5059-5066, 2020.

[4] Han J-S, Chang JW, and Han J-H. The advance ratio effect on the lift augmentations of an insect-like flapping wing in forward flight. *Journal of Fluid Mechanics,* Vol. 808, pp. 485-510, 2016.

[5] Addo-Akoto R, Han J-S, and Han J-H. Influence of aspect ratio on wing–wake interaction for flapping wing in hover. *Experiments in Fluids,* Vol. 60, No. 11, pp. 1-18, 2019.

[6] Han J-S, Kim J-K, Chang JW, and Han J-H. An improved quasi-steady aerodynamic model for insect wings that considers movement of the center of pressure. *Bioinspiration & biomimetics,* Vol. 10, No. 4, p. 046014, 2015.

[7] Nguyen AT, Kim J-K, Han J-S, and Han J-H. Extended unsteady vortex-lattice method for insect flapping wings. *Journal of Aircraft,* Vol. 53, No. 6, pp. 1709-1718, 2016.

[8] Nguyen AT, Tran ND, Vu TT, Pham TD, Vu QT, and Han J-H. A neural-network-based approach to study the

energy-optimal hovering wing kinematics of a bionic hawkmoth model. *Journal of Bionic Engineering,* Vol. 16, No. 5, pp. 904-915, 2019.

[9] Berman GJ and Wang ZJ. Energy-minimizing kinematics in hovering insect flight. *Journal of Fluid Mechanics,* Vol. 582, pp. 153-168, 2007.

[10]Kurdi M, Stanford B, and Beran P. Kinematic optimization of insect flight for minimum mechanical power. *AIAA paper,* Vol. 1420, p. 2010, 2010.

[11]Ghommem M *et al.* Global optimization of actively morphing flapping wings. *Journal of Fluids and Structures,* Vol. 33, pp. 210-228, 2012.

[12]Nguyen AT, Le VDT, Duc V, and Phung VB. Study of vertically ascending flight of a hawkmoth model. *Acta Mechanica Sinica,* Vol. 36, No. 5, pp. 1031-1045, 2020.

[13]Willmott AP and Ellington CP. The mechanics of flight in the hawkmoth Manduca sexta. I. Kinematics of hovering and forward flight. *The Journal of experimental biology,* Vol. 200, No. 21, pp. 2705-2722, 1997.

[14]Nguyen AT, Han J-S, and Han J-H. Effect of body aerodynamics on the dynamic flight stability of the hawkmoth Manduca sexta. *Bioinspiration & biomimetics,* Vol. 12, No. 1, p. 016007, 2016.

[15]Kim J-K, Han J-S, Lee J-S, and Han J-H. Hovering and forward flight of the hawkmoth Manduca sexta: trim search and 6-DOF dynamic stability characterization. *Bioinspiration & biomimetics,* Vol. 10, No. 5, p. 056012, 2015.

[16]Wissa BE, Elshafei KO, and El-Badawy AA. Lyapunov-based control and trajectory tracking of a 6-DOF flapping wing micro aerial vehicle. *Nonlinear Dynamics,* Vol. 99, No. 4, pp. 2919-2938, 2020.

[17]Kalliny AN, El-Badawy AA, and Elkhamisy SM. Command-filtered integral backstepping control of longitudinal flapping-wing flight. *Journal of Guidance, Control, and Dynamics,* Vol. 41, No. 7, pp. 1556-1568, 2018.